Preparation and characterization of nanorod-like TiO2 and ZnO films used for charge-transport buffer layers in P3HT based organic solar cells

Tran Thi Thao, Dang Dinh Long, Vo-Van Truong, and Nguyen Nang Dinh

Citation: AIP Conference Proceedings **1763**, 030002 (2016); doi: 10.1063/1.4961346
View online: http://dx.doi.org/10.1063/1.4961346
View Table of Contents: http://scitation.aip.org/content/aip/proceeding/aipcp/1763?ver=pdfcov
Published by the AIP Publishing

Preparation and Characterization of Nanorod-like TiO_2 and ZnO Films used for Charge-Transport Buffer Layers in P3HT Based Organic Solar Cells

Tran Thi Thao[1], Dang Dinh Long[1],Vo-Van Truong[2], Nguyen Nang Dinh[1,a)]

[1]*University of Engineering and Technology, Vietnam National university Hanoi*
144, Xuan Thuy, Hanoi 1000, Vietnam
[2]*Department of Physics, Concordia University, 1455 de Maisonneuve Blvd W, Montreal (Quebec)*
Canada H3G 1M8

[a)]*Corresponding author: dinhnn@vnu.edu.vn*

Abstract. With the aim of findingout the appropriate buffer layers for organic solar cells (OSC), TiO_2 and ZnO on ITO/glass were prepared as nanorod-like thin films. The TiO_2 films were crystallyzed in the anatase phase and the ZnO films, in the wurtzite structure. The nanorods in both the fims have a similar size of 15 to 20 nm in diameter and 30 to 50 nm in length. The nanorods have an orientation nearly perpendicular to the ITO-substrate surface. From UV-Vis data the bandgap of the TiO_2 and ZnO films were determined tobe 3.26 eV and 3.42 eV, respectively. The laminar organic solar cells with added TiO_2 and ZnO, namely ITO/TiO_2/P3HT:PCBM/LiF/Al (TBD) and ITO/ZnO/P3HT:PCBM/LiF/Al (ZBD)were made for characterization of the energy conversion performance. As a result, comparing to TiO_2,the nanorod-likeZnO filmwas found to be a much better buffer layer that made the fill factor improve from a value of 0.60 for TBD to 0.82 for ZBD, and consequently thePCE was enhanced from 0.84 for TBD to 1.17% for ZBD.

INTRODUCTION

In recent years, photovoltaic devices based on polymeric and organic materials have been increasingly investigated because of their reduced fabrication cost and less complicated technology than the inorganic devices. Preparation and characterization of several nanocomposite solar cells made from blends of polymers and fullerene materials were reportedelsewhere.[1-4]It is seen that the photoelectric conversion efficiency (PCE) of such organic solar cells (OSCs) is still low because of the limited charge-separation efficiency of the organic-fullerene blend structure. By embedding inorganic nanocrystalline particles like TiO_2 and ZnO into organic matrices one can enhance the PCE of the devices. TiO_2 and ZnO can be considered as n-type of wide bandgap semiconductors. In order to take advantage of the absorbance of a polymeric photoactive material, TiO_2 nanotubes or nanorods were mixed in conjugate polymers, f.i. poly(3-hexylthiophene)(P3HT)[5] and Poly[2-methoxy-5-(2'-ethyl-hexyloxy)-1,4-phenylene vinylene] (MEH-PPV).[6]Comparing with inorganic photoactive material like Si, where there are homogenous p-n junctions, polymeric photoactive materials contain all heterojunctions that cause the strong decay of the excitons which are generated in the donors/acceptors junctions under the illumination of solar radiation. This results in the lowering of the PCE of the solar cells. The exciton decay can be diminished by adding the so-called charge transport buffer layers sandwiched between electrodes and photoactive layers. With the appropriate energy bandgaps compared to the electrodes and photoactive layer in OSCs, the buffer layers can favor a stronger charge separation, consequently the generated charge carriers (i.e. electrons and holes) more efficiently move to opposite directions. By this way the performance parameters of the OSCs such as open-circuit voltage (V_{oc}), short-circuit current (J_{sc}), fill factor (*FF*) and finally *PCE* can be enhanced.

Frontiers in Materials Science (FMS2015)
AIP Conf. Proc. 1763, 030002-1–030002-8; doi: 10.1063/1.4961346
Published by AIP Publishing. 978-0-7354-1421-1/$30.00

This work presents results of our recent research on the preparation and characterization of TiO_2 and ZnO thin films used as buffer layers in P3HT-based OSCs. The comparison of the photoelectric conversion performance of the OSCs with TiO_2 and ZnO buffer layers is also presented.

EXPERIMENTAL

A. Preparation of nanorod-like $TiO_2$and ZnO thin films

To prepare TiO_2 films on ITO (TiO_2/ITO),an anodic electrodeposition technique has been used following the process reported in.[7]A 300-mm-thick ITO-coated glass having a sheet resistance of 10 Ω and a transmittance of 90% has been used as substrate. The ITO/glass substrates were ultrasonically cleaned in distilled water, followed by cleaning in ethanol and acetone. An anodic current density of 0.25 mA/cm^2 was applied to the ITO/glass electrode. The electrolyte with pH = 2.5 was prepared by mixing 25 % solution of $TiCl_3$ in 3 % HCl, adding Na_2CO_3 solution to adjust the pH. The deposition time was from 30 to 60 min. Electrodeposition was carried out on a AUTOLAB-Potentiostat PGS-30) using the three-compartment cell where ITO/glass was used as the working electrode (WE), a saturated calomel electrode (SCE) was used as the reference electrode and a platinum grid was the counter electrode (CE).

Deposition of nanorod-like ZnO films on ITO/glass substrates was carried out on the same AUTOLAB-Potentiostat PGS-30 with the three above mentioned electrodes. The electrolyte for deposition was prepared from a100 ml of zinc nitrate Zn $(NO_3)_2$. $6H_2O$ and 100 ml of hexamethylenetetramine $C_6H_{12}N_4$solution, adding H_2O to adjust a total volume solution of 500 ml. The electrochemical process took place at room temperature with an anodic current density of 0.35 mA/cm^2, the deposition time was from 45 to 90 min. As-deposited TiO_2 and ZnO films were rinsed in de-ionized water, then annealed in air at 450^{o}C for 3 h.

B. Device preparation

To deposit the photoactive layers on TiO_2/ITO and ZnO/ITO, a mixture of poly(3-hexylthiophene) (P3HT) and [6,6]-phenyl C_{61}-butyric acid methyl ester (PCBM) as 1:1 volume ratio (abbreviated to P3HT:PCBM) solution used for spin-coating was prepared by dissolving 8 mg of P3HTpowders in 10 ml of chlorobenzene, then adding 8 mg of PCBM. To prepare a homogenous dispersion of PCBM in P3HT, the solution was well mixed for 8 h by using magnetic stirring. The conditions for spin-coating P3HT:PCBM/TiO_2/ITO and P3HT:PCBM/ZnO/ITO were similar to that reported in,[5] namely: a delay time of 120 s, a rest time of 30s, a spin speed of 1500 rpm, and an acceleration of 500 rpm, and finally a drying time of 2 min. The thickness of the P3HT:PCBM was about 100 nm. The samples were put in a flow of dried gaseous nitrogen for 12 hours. As electrodes, an ITO/glass on one side and a 50-nm thick LiF/Al bilayer contact on the other side were used. Using a mask with windows of 3 mm × 5 mm in size (the active area of a cell was 0.15 cm^2), the LiF/Al electrode (shallow contact) onto P3HT:PCBM/TiO_2/ITO was successivelyevaporatedin a vacuum of 1.33×10^{-3} Pa. With a thin LiF layer one can ensure a good ohmic contact between the P3HT (polymer) and Al (inorganic) layers.[8]Finally, two types of the devices with respective structures of ITO/TiO_2/P3HT:PCBM/LiF/Al and ITO/ZnO/P3HT:PTC/LiF/Al were prepared and respectively called “TBO” and “ZBO”, for subsequent discussion.

The surface morphology was studied using a Hitachi “S- 4800” field-emission scanning electron microscope (FE-SEM). X-ray diffraction analysis (XRD) was done on a Brucker “Advance-8D” X-ray diffractometer. Optical absorption and Photoluminescence measurements were carried out using a JASCO ultraviolet–visible-near infrared (UV-Vis-NIR) “V-570” spectrophotometer and a Flouromax-4 spectrofluorometer. Measurements of the device parameters such as the open-circuit voltage, $V_{oc;}$ the short-circuit current density, J_{sc}; and the fill factor (*FF*) were carried out on an Auto Lab-Potentiostat PGS-30 electrochemical unit connected to "Sol 1A" Newport source which provided an energy spectrum similar to the AM1.5 - 100 mW/cm^2 solar-illumination.

III. RESULTS AND DISCUSSIONS

A. Structural and optical properties of TiO_2 and ZnO films

Figure 1 shows typical scanning electron micrographs (FE-SEM) of nanorod-like TiO_2 and ZnO films deposited on ITO/glass substrates. Both the two films are nano-porous with orientated nanorod arrays. The rods of the two different materials stand almost perpendicular to the substrate, having a similar diameter in nanoscale, in the range of 15 to 20 nm, and being about 40 to 50 nm in length. Polymeric composites serving as a photoactive layer were then spin-coated on these films to get the OSC devices. With such porous structures of the films, during the spinning process, the nanorods can adhere by strong electrostatic forces to the photoactive layer and between themselves, and capillary forces can then draw the polymeric solution around the nanorods into cavities without pinholes through the layers. This results in the elimination of nano-cracks as charge carriers traps that were often formed in the pure conjugate polymer films during annealing as observed in a recent work.[5]

The X-ray diffraction pattern of TiO_2 and ZnO films were shown on Fig. 2. There are five large diffraction peaks at (101), (002), (021), (102) and(202); and three small peaks at (200), (112) and (113) for the TiO_2 film (Fig 2a). Four large peaks at (100), (101), (102), (110) and one peak at (103) were observed for the ZnO film (Fig 2b). Those are the crystal structure of the anatase TiO_2[9] and wurtzite ZnO phase[10], respectively.

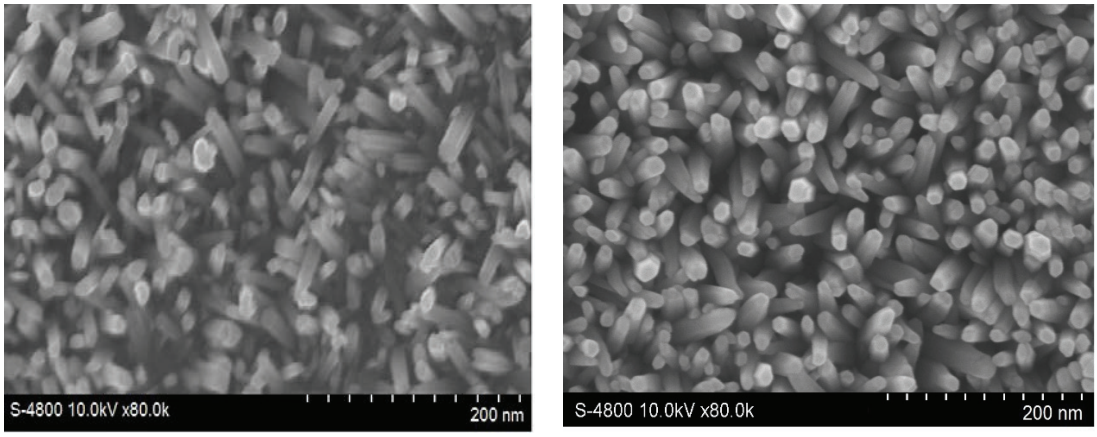

(a) **(b)**

FIGURE 1. FE-SEM micrograph of the TiO_2/ITO glass (a) and ZnO/ITO/glass thin films (b). The thickness of both films is 50 - 70 nm.

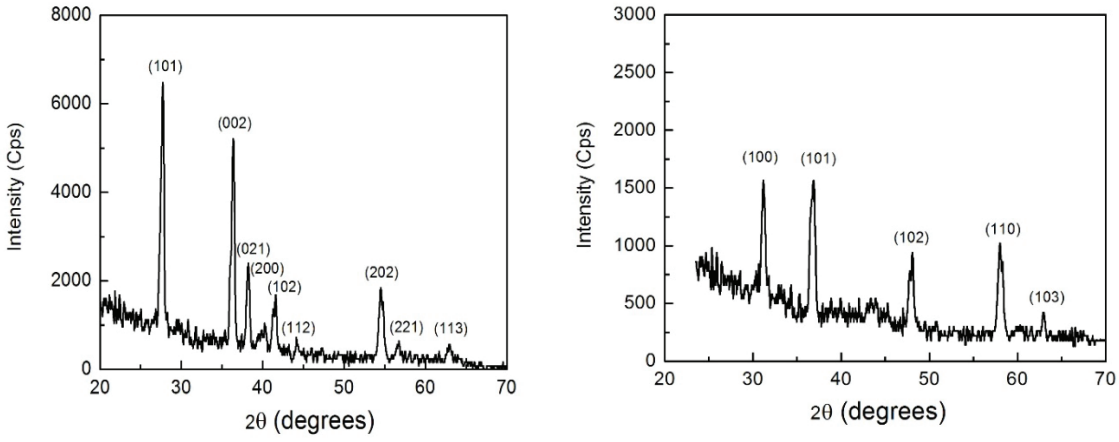

FIGURE. 2. X-ray diffraction patterns of the TiO_2/ITO (a) and ZnO/ITO (b).

The fact that the peak width is rather large shows that both the $TiO_2$and ZnO films consist of small particles. To avoid the effect of broadening peaks due to X-ray instrument, we used a scanning rate of the X-ray detector as small as 0.25^o/s. Moreover, for the crystalline rods the lattice is similar to the one of a single crystal, the peak broadening due to the lattice strain can be eliminated. Thus one can use Scherrer formula to determine the size (R) for the crystalline rods:

$$R = \frac{0.9\lambda}{\beta cos\theta} \tag{1}$$

whereλ is wavelength of the X-ray used (λ = 0.15406 nm), β the peak width of half height in radians and θ the Bragg angle of the considered diffraction peak.[11]

The value β determined from all the peaks of the XRD patterns of both films (Fig. 2) was found to be in a range of 0.008 to 0.015 radian, thus the size of the nanorod-like particles of both TiO_2 and ZnO films determined by Eq. (1)was in range of 12 to 18 nm. Since the XRD patterns revealed the diffraction of the lattice of crystalline grains, the FE-SEM showed the morphology of separate particles (or rods) that may contain a few grains. But, in our work the grain size determined from XRD patterns was consistent with the particle size measured from FE-SEM, the nanorods of both the TiO_2 and ZnO can thus be seen as monocrystalline rods with slightly different orientations.

Transmittance spectra of the TiO_2 and ZnO films are shown in Fig. 3.From this figure one can see that in comparison with TiO_2 film, ZnO film possesses higher transmittance. Indeed, at the wavelength of 500 nm the transmittance of ZnO reached a value ~90 % which is about 6% larger than that of TiO_2. Moreover, ZnO film has a 30 nm wider range in the short wavelengths where a part of solar radiation can go though.

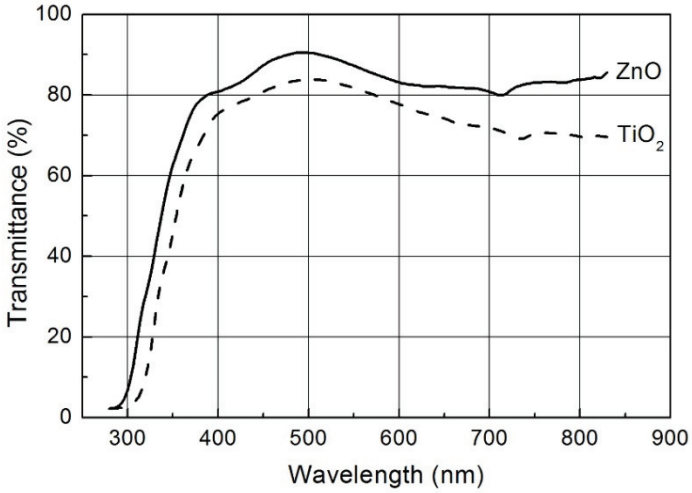

FIGURE 3. Transmittance spectra of aZnO nanorods/glass sample (solid line) and a TiO_2 nanorods/glass sample (dotted line).

Indeed, the main factors that affect the absorption of the TiO_2 and ZnO films are their components and structures. The relationship between the absorption coefficient and the concentration of free carries is expressed as:[12]

$$\alpha = \frac{(N_e)^2\lambda_o^2}{8m^*\pi^2nc^3\tau} \tag{2}$$

whereα is the absorption coefficient, N_e is the concentration of free carriers, n is the refractive index, m^* is the effective mass of free carriers, λ_0 is the absorption wavelength, τ is the relaxation time and c is the speed of light. Since the value in magnitude of n, m^* and τ of TiO_2 and ZnO are not much different, one can qualitativelysuggest that the absorption coefficient of TiO_2 and ZnO thin films is strongly dependent on the concentration of free carriers. At room temperature, the TiO_2 film has a free carrier concentration ($10^{19}cm^{-3}$)[13] larger than that the ZnO film (10^{17} cm^{-3}).[14]Thus the absorption coefficient of the TiO_2film is larger than the one of the ZnO film. This results in larger transmittance spectra of ZnO film than TiO_2(Fig 3).

UV-Vis data at short wavelength can be used to estimate the energy gap, E_g, of the films by using the expression:[15]

$$\alpha h\nu = A\left(h\nu - E_g\right)^n \tag{3}$$

where h is Planck's constant, ν is the frequency of the incident UV-Vis radiation, A is a constant and n is 1/2 for direct band semiconductors and 2 for indirect band gap semiconductors. A graph is plotted between $(\alpha h\nu)^2$ or the square of $(\alpha h\nu)$ and $\alpha h\nu$ (as abscissa), and a straight line is obtained. From the extrapolation of the straight line to $(\alpha h\nu)^2$ and/or $(\alpha h\nu)^{1/2} = 0$ axis one can determine the bandgap of the investigated sample. As expected, best fits were obtained for n=2 (indirect band) for both the TiO_2 and ZnO. Thus from our experiments, the energy gap of nanorod-like TiO_2 and ZnO films was found to be of approximately 3.26 eV and 3.42 eV, respectively (Fig. 4).

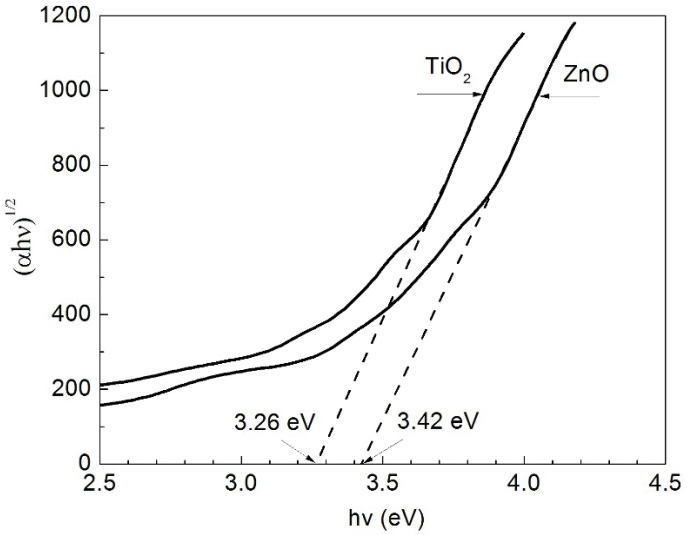

FIGURE 4. Bandgap determination of TiO_2 and ZnO films

The gap energies calculated from UV-VIS data were not much larger than the gap energy of bulk samples, which is in the range of 3.0 to 3.2 eV for TiO_2[16] and 3.1 to 3.3 eV for ZnO.[17]In the next section we present the photoelectric conversion of P3HT based OSC devices with added TiO_2 and ZnO buffer layers, and comparison of their efficiency performance.

B. Photoelectric conversion performance of OSCs with buffer layers

Figure 5 shows plots of *J-V* characteristics obtained for two devices, TBD and ZBD, under an illumination with a power density of 100 mW/cm^2. The larger *FF*, the more charge carriers will reach the electrodes. In fact, there is a competition between charge carrier recombination and transport which is dependent on the charge separation. The *FF* can be determined by:

$$FF = \frac{(J\times V)max}{J_{sc}\times V_{oc}} \tag{4}$$

where $(J\times V)_{max}$ is the rectangle having the largest area. Then the PCE is determined by:

$$PCE = \frac{FF\times J_{sc}\times V_{oc}}{P_{in}} \tag{5}$$

where $P_{in}$is the illuminating power density, in mW/cm^2. In our experiments, P_{in}= 100mW/cm^2.

It is seen that V_{oc} and J_{sc} can be taken from the *J-V* curves (as shown by the arrows in the plots, Fig. 5). All the performance parameters of the two OSCs, namely V_{oc}, J_{sc}, *FF* and *PCE* that were calculated by Eq. (4) and Eq. (5) are listed in Table 1.The *PCE* of the ZBD cell are compatible to the one for a cell using ZnO buffer layer (ITO/ZnO/C60/PAT6/Au) that was obtained by Hori at al.[19] It is seen that V_{oc} of the ZBD cell is not much larger than the one of TBD (namely 0.72 V compared to 0.65 V), but J_{sc} of TBD is larger than that of the TBD cell (2.15 mA/cm^2 as compared to 1.98 mA/cm^2). From Fig. 5 one can see that the relative lowering of the J_{sc} of ZBD cell (compared to TBD) is compensated by a relative increase of itsV_{oc}. Thus, the larger PCE of the ZBD compared to the TDB cell can be attributed to the enhancement of its fill factor: FF_{ZBD} (0.82) is much larger than FF_{TDB}(0.60).

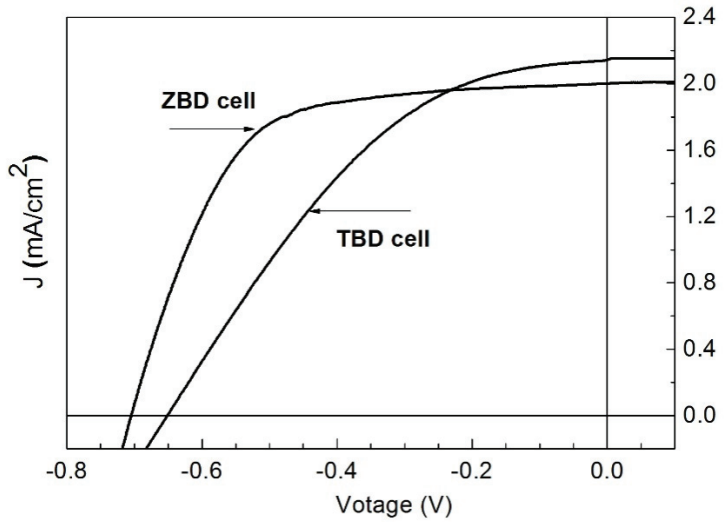

FIGURE 5.J-V characteristics obtained in the illumination regime for the cells with a structure of ITO/PEDOT/P3HT:PCBM/LiF/Al (OSC-1) and ITO/PEDOT/P3HT:PTC/LiF/Al (OSC-2).

TABLE 1. Solar cell data for TBD and ZBD devices.

	Area (cm^2)	***V*$_{oc}$(mV)**	***J*$_{sc}$(mA/cm^2)**	***FF***	***PCE* (%)**
TBD	0.15	650	2.15	0.60	0.84
ZBD	0.15	720	1.98	0.82	1.17

The improvement in the FF of the ZBD cell can be explained due to optical properties as well as the relative energy band structures of the multiple layers in the devices. The schematic drawing in Fig. 6 is similar to that shown by Hori at al.[19]The energy band gap (E_g) of P3HT, PCBM, TiO_2 and ZnO is ca. 2.0, 2.3, 3.2 and 3.4 eV, respectively. The difference between conducting band level of TiO_2 and ZnO and the lowest unoccupied molecular orbital (LUMO) level of PCBM is similar and equal to ΔE = 0.8 eV.

When the polymer/inorganic heterojunctions were excited by photons, excitons appeared in the polymer as generated electrons jumped from the highest unoccupied molecular orbital (HOMO) to the LUMO. In comparison with TiO_2, the bandgap, E_g, of the ZnO buffer layer is larger and the transmittance is higher in a larger range of wavelengths(see Fig.3 and Fig. 4). Due to the higher transmittance, a larger number of the photons from the solar illumination went through the buffer layer to excite the photoactive layer, consequently more charges generated. With such a large E_g and a deep valence-band level of ZnO and TiO_2compared to the HOMO level of PCBM, namely ΔE_1= 1.9 eV and ΔE_2=1.7 eV, respectively (Fig. 6),there is no energy barrier for electrons, but a high energy barrier for holes exists at the interface of ZnO/PCBM and TiO_2/PCBM. This results in favoring generated electrons moving to the ITO electrode, whereas holes generated in the photoactive layer (P3HT:PCBM) are blocked at the ZnO/PCBM interface or TiO_2/PCBM. Since $\Delta E_1 > \Delta E_2$upon inserting the ZnO buffer layer, the charge separation becomes stronger when TiO_2 is used for the buffer layer. Under the intensive internal electrical field of the organic

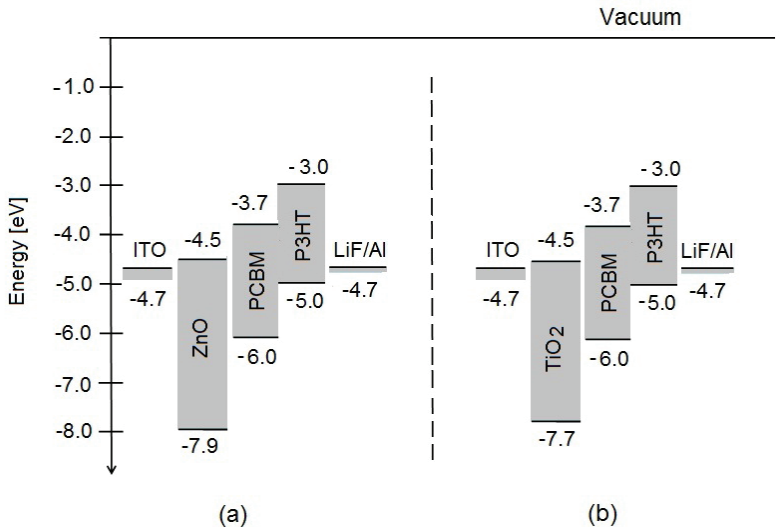

FIGURE 6. Schematic energy levels of ITO, ZnO or TiO_2, P3HT:PCBM, LiF/Al. This diagram illustrates the band structure of ZnO (a) and TiO_2 (b) relative to the HOMO and LUMO energy levels of the P3HT:PCBM compared to the vacuum level.

photoactive layer, the separate electrons and holes easily move to the opposite directions, reaching electrodes. In case of the ZnO buffer layer, a larger amount of the charge carriers reached the electrodes of the cells.

IV. CONCLUSION

The nanorod-like TiO_2 and ZnO thin films onto ITO/glass were prepared by a sol-gel and electrochemical method. The TiO_2films were crystallizedin the anatase phase and theZnO films, in the wurtzite structure. The nanorods in both films have a similar size of 15 to 20 nm in diameter and 30 to 50 nm in length. The nanorods have an orientation nearly perpendicular to the ITO-substrate surface. With a high transmittance and a large bandgap determined from the UV-VIS data, both the ZnO and TiO_2 films were used for the electron buffer layers in laminar organic solar cells, ITO/ZnO/P3HT:PCBM/LiF/Al (ZBD) and ITO/TiO_2/P3HT:PCBM/LiF/Al (TBD). Comparing with TiO_2, ZnO formed a much better electron buffer layer that made the fill factor increase to 0.82 from 0.60 for TiO_2, and consequently the photoelectric conversion efficiency was improved from 0.84 to 1.17%. The nature and nanostructures of a buffer layer can thus influence greatly the performance of OSCs.

ACKNOWLEDGEMENTS

This research was funded by the Vietnam National Foundation for Science and Technology (NAFOSTED) under grant number 103.02-2013.39. Infrastructure and equipment provided for sample preparation, FE-SEM, XRD patterns, absorption and PL spectra, solar cell performance measurements were made possible in the VNU project on “Nanotechnology and Applications” supported by the Vietnamese Government.

REFERENCES

1. G.Yu, J.Gao,J.C. Hummenlen, and F.Wudl, A.J. Heeger, Science**270**, 1789–1791 (1995).
2. S.E. Shaheen, C.J. Brabec, N.S. Sariciftci, F. Padinger, T.Fromherz, and J.C. Hummenlen, Appl. Phys.Lett. **78**, 841–844 (2001).
3. P. Schilinsky, C. Waldauf, and C.J. Brabec, Appl. Phys.Lett. **81**, 3885–3887 (2002).

4. M.M. Wienk, J.M. Kroon, W.J.H Verhees, J. Knol, J.C. Hummenlen, P.A. van Hal, and R.A. J. Janssen, Angew. Chem. Int. Ed. **42**, 3371–3375 (2003).
5. T. T. Thao, T. Q. Trung, V-V. Truong, and N. N. Dinh, J. Nanomaterials**2015**, Article ID 463565,7p (2015).
6. K. Kawata, V. M. Burlakov, M. J. Carey, H. E. Assender, G. A. D. Briggs, A. Ruseckas, and I. D. W. Samuel, Sol. Energ. Mat. Sol. Cells **87**, 715–724 (2005).
7. F. Cherkaoui El Moursli, A. Douayr, F. Hajji, K. Nouneh, A. Guessous, K. Nabih, A. Hadri, and M. Abd-Lefdil, Sensors & Transducers **27**, Special Issue, 137–141 (2014).
8. N. N. Dinh, L. H. Chi, T. T. C. Thuy, T. Q. Trung, and V-V. Truong, J. Appl. Phys. **105**,093518-1÷093518-5 (2009).
9. H. G. Yang and H. C. Zeng. J. Phys. Chem. B **108**, 3492–3495 (2004).
10. S. Fujihara, C. Sasaki, and T. Kimura, Appl. Surf. Sci. **180**, 341–350 (2001).
11. B. D. Cullity, Elements of X-Ray Diffraction, 2nd. Ed. (Addison-Wesley, Reading, MA, 1978) p. 102.
12. J. X. Fang and D. Lu, Solid State Physics (Shanghai Technology and Science Press, Shanghai, 1980) p. 108.
13. H. Tang, K. Prasad, R. Sanjinès, P. E. Schmid, and F. Lévy, J. Appl. Phys. **75**, 2042–2047 (1994).
14. K. Thonke, Th. Gruber, N. Teofilov, R. Schönfelder, A. Waag, R. Sauer, Physica B **308–310**, 945–948 (2001).
15. J. Tauc, in: "Amorphous and liquid semiconductors" edited by J. Tauc (Plenum Press, London and NewYork, 1974) p. 159.
16. H. Lin, C. P. Huang, W. Li, C. Ni, S. I. Shah, and Y-H. Tseng, Applied Catalysis B: Appl. Catal. B-Environ. **68**, 1–11(2006).
17. M. Matsumura and R. P. Camata, Thin Solid Films **476**, 317–323 (2005).
18. E. Brus, J. Chem. Phys. **90**, 2555–2560 (1986).
19. T. Hori, H. Moritou, N. Fukuoka, J. Sakamoto, A. Fujii, and M. Ozaki, Materials**3**, 4915–4921 (2010).